CANADIAN JOURNAL OF RESEARCH

VOLUME 27 SEPTEMBER, 1949 NUMBER 5

— SECTION A —

PHYSICAL SCIENCES

Contents

NATIONAL RESEARCH COUNCIL
OTTAWA, CANADA

CANADIAN JOURNAL OF RESEARCH

The *Canadian Journal of Research* is issued in six sections, as follows:

A. Physical Sciences	D. Zoological Sciences
B. Chemical Sciences	E. Medical Sciences
C. Botanical Sciences	F. Technology

For the present, Sections A, C, D, and E are to be issued six times annually, and Sections B and F, twelve times annually, each under separate cover. with separate pagination.

The *Canadian Journal of Research* is published by the National Research Council of Canada under authority of the Chairman of the Committee of the Privy Council on Scientific and Industrial Research. The *Canadian Journal of Research* is edited by a joint Editorial Board consisting of members of the National Research Council of Canada, the Royal Society of Canada, and the Chemical Institute of Canada.

Sections B and F of the *Canadian Journal of Research* have been chosen by the Chemical Institute of Canada as its medium of publication for scientific papers.

Manuscripts should be addressed:

Editor-in-Chief,
Canadian Journal of Research,
National Research Council, Ottawa, Canada.

* *Deceased.*

CANADIAN JOURNAL OF RESEARCH

The *Canadian Journal of Research* is issued in six sections, as follows:

A. Physical Sciences	D. Zoological Sciences
B. Chemical Sciences	E. Medical Sciences
C. Botanical Sciences	F. Technology

For the present, Sections A, C, D, and E are to be issued six times annually, and Sections B and F, twelve times annually, each under separate cover. with separate pagination.

The *Canadian Journal of Research* is published by the National Research Council of Canada under authority of the Chairman of the Committee of the Privy Council on Scientific and Industrial Research. The *Canadian Journal of Research* is edited by a joint Editorial Board consisting of members of the National Research Council of Canada, the Royal Society of Canada, and the Chemical Institute of Canada.

Sections B and F of the *Canadian Journal of Research* have been chosen by the Chemical Institute of Canada as its medium of publication for scientific papers.

EDITORIAL BOARD

EDITORIAL COMMITTEE

Manuscripts should be addressed:

Editor-in-Chief,
Canadian Journal of Research,
National Research Council, Ottawa, Canada.

* *Deceased.*

Canadian Journal of Research

Issued by THE NATIONAL RESEARCH COUNCIL OF CANADA

VOL. 27, SEC. A. SEPTEMBER, 1949 NUMBER 5

WAVE LENGTHS, EQUIVALENT WIDTHS, AND LINE PROFILES IN THE SPECTRUM OF THE STAR H.D. 190073[1]

BY C. S. BEALS AND MIRIAM S. BURLAND

Abstract

With the aid of long exposures (18 and 25 hr. respectively) the spectrum of H.D. 190073 in the ordinary region has been photographed with dispersions of 7.3 to 15.2 Å per mm. The resulting spectrograms revealed approximately 100 stellar lines not observed with single-prism dispersion as well as indicating more clearly the structure of a number of complex line profiles. Wave lengths, identifications, and equivalent widths are listed for all observed lines, and a number of the more interesting line profiles are illustrated. The interpretation of line profiles is discussed and it is pointed out that the presence of asymmetrical hydrogen lines is an indication of a shell of relatively small diameter.

Introduction

The spectrum of the emission line star H.D. 190073 (α 1900 19^h $58.^m1$, δ 1900 + 5° 28′ mag. 7.9 AOe) is, in a number of respects, unique in the sky because of the peculiar character of its emission and absorption lines. Studies of its spectral characteristics have been made by Merrill (6), Beals (2, 3) and Struve and Swings (8).

The spectrum is characterized by emission lines due to hydrogen, neutral sodium, and ionized metals such as CaII, FeII, TiII, etc. A number of the lines have a P Cygni character and in the case of hydrogen the line profiles exhibit definite variability. The forms of the lines due to CaII in this spectrum are unusually intricate and complex, while H.D. 190073 is one of the few stars that exhibit well marked emission due to neutral sodium.

In spite of the fact that the star has been studied by several investigators and that a number of efforts have been made to work out detailed explanations of a number of its unusual features, its spectrum remains a puzzle that in the main has not been solved. The present study was undertaken with the hope of making a worth while contribution to our knowledge of this spectrum by investigating it with higher dispersion than had hitherto been employed.

The Observations

The spectrograms and microphotometer tracings on which this study is based were secured by one of the authors (Beals) at the Dominion Astrophysical Observatory at Victoria, B.C., before his transfer to Ottawa.

[1] *Manuscript received May 10, 1949.*

Vol. 2. No. 4. Contributions from the Dominion Observatory. Published by permission of the Director, Mines, Forests and Scientific Services Branch, Department of Mines and Resources, Ottawa, Canada.

Previous studies of the star at Victoria were made with single-prism dispersion in the ordinary region and three prisms in the visible. The values of spectrographic dispersions used in these earlier studies, as well as in the present work, are given in Table I. Seventeen spectra were secured in all, four in the visible λ 5500–6700 and thirteen in the ordinary photographic region λ 3850–5000.

TABLE I

Dispersing system	Camera focal length, cm.	Symbol	Dispersion, Å/mm.	
			λ 3933	λ 4340
I-Prism	96	IL	14.6	22.1
	71	IM	19.9	30.3
	42	IS	33.5	50.8
II-Prism	96	IIL	7.3	11.0
	71	IIM	10.0	15.2
			λ 5875	λ 6563
III-Prism	71	IIIM	34.5	46.0

A careful examination of the best of the single-prism spectrograms gave indication of many faint narrow lines of an intensity close to the limit of visibility, and there seemed reason to believe that studies with higher dispersion might well reveal many more lines. It also appeared probable that increased dispersion would yield additional information regarding the peculiar emission and absorption line profiles due to CaII and hydrogen as well as those of other atoms. The exposure time required to secure a II. single-prism spectrogram of dispersion 22 Å per mm. at H_γ, well exposed in the region of λ 3933, was approximately six hours. For a star of the declination of H.D. 190073 this represents an all night exposure and it was clear that several nights would be required in order to secure good plates with the higher dispersion given by two prisms. Some risks of failure are involved in such long exposures and they are of course very prodigal of observing time but it was considered that the importance of the problem warranted the attempt.

An exposure was accordingly begun on the night of July 23, 1946, and continued through three nights including July 25. The total exposure was 17 hr. and 41 min. The long focus (96 cm.) camera was used with two prisms and this combination gives a dispersion of 7.3 Å per mm. at λ 3933 and 11.0 Å per mm. at H_γ. The temperature of the spectrograph was maintained at a uniform level by means of a thermostat. Some trouble was experienced on one night owing to a sudden drastic rise in the outside temperature, but it was found possible to exercise the necessary control by the use of a damp sheet covering the spectrograph and bags of dry ice symmetrically distributed about the spectrograph frame. The plateholders were firmly clamped into place so that at the end of a night's work it was possible to replace the dark

slide without jarring the plate. Suitably spaced exposures of the iron arc were made on each night, and while the images of the iron lines on the plates showed evidence of a certain amount of flexure at right angles to the dispersion, the lines were of good definition and there was little evidence that temperature or flexure effects had seriously interfered with the purity of the spectrum.

The star spectrum was of a good density in the region of λ 3968–λ 4500 and many fine metallic lines were clearly visible. In the region of the K line (λ 3933), however, the exposure was weak and it was decided to make another exposure of longer duration using a camera of shorter focal length (71 cm.) in the hope of getting adequate exposures at the bottoms of the very strong H and K lines of CaII. The second exposure was begun on August 6 and continued through August 9 with a total exposure time of 24 hr., 56 min. The result was a plate beautifully exposed in the H and K region and well usable throughout the entire range λ 3896–λ 4600. Illustrations of the spectra are shown in Plate I.

The present paper contains information on wave lengths, identifications, and line intensities from the two-prism spectrograms described above, as well as from a number of earlier single-prism plates of comparable quality but smaller dispersion.

Wave Length Measurements

For the determination of wave length, both direct micrometer measures of the plates as well as microphotometer tracings were used. The tracings were made on the Victoria microphotometer (1) and were of ×100 magnification. Each tracing had superimposed upon it a record of both sets of iron comparison lines in addition to the star spectrum. The measurement of the tracings for wave length was carried out on a small micrometer machine specially designed for this purpose and loaned to the writers by the Dominion Astrophysicist, Dr. J. A. Pearce. The character of the machine is illustrated in Plate II. The motion of the tracing is governed by the rotation of a precision roller with a micrometer head on one end, and the accuracy with which the position of a line of the star or comparison spectrum can be read is 0.2 mm. on the tracing, corresponding to 0.002 mm. on the plate. While this may not look like extreme precision, since plate settings can be made to 0.0005 mm., it may be pointed out that settings on the tracings can be repeated with greater consistency than on the plates and the over-all accuracy is probably about the same. The advantage of the use of both methods is that it helps to eliminate spurious lines, while for the numerous peculiar line profiles in the spectrum of H.D. 190073 the part of the line involved in the setting is more definitely known when it is seen on a microphotometer tracing. In forming means, equal weight was given to measures of plates and tracings and in general the agreement between the two types of measurements was good.

In the reduction of the measures and the computation of wave lengths the ordinary Hartmann formula for prismatic dispersion was used in conjunction with correction curves derived from the iron comparison lines. Since the

radial velocity of the star is not large and since it is impossible to be certain that such line displacements as occur are not due to motions in the star's atmosphere, the wave lengths are published without correction for velocity effects other than that of the earth's motion. The intrinsic motion of the star and any Doppler effects within its atmosphere are therefore contained in the wave lengths of Table II.

When the list of wave lengths from the two high-dispersion plates was completed, it was compared with an earlier list derived from four single-prism plates by Beals. As might be expected there were some discrepancies and a very careful line by line comparison was made not only between the one-and two-prism plates, but between the corresponding tracings as well. It was found that in some instances lines that appeared as single on the one-prism plates were actually of multiple character when observed with the higher dispersion. Some lines of definitely spurious character were eliminated and it was found that on the larger dispersion plates there were recorded an additional 100 lines that did not appear on the single-prism spectrograms.

Identification of Lines

For the identification of lines, main reliance was placed on Mrs. Moore-Sitterly's New Table of Multiplets (7) although much initial labor was saved by consulting Wyse's (9) list of wave lengths in the spectrum of α Cygni.

A study of Table II indicates that, apart from the Balmer series of hydrogen, all the identifications suggested for the wave lengths of H.D. 190073 are lines of neutral and singly ionized metals. Apart from the CaII doublet, which is a very conspicuous feature of the spectrum, ionized iron and titanium are responsible for the strongest emission lines. It was at first considered that FeI appeared in absorption only, but as will be mentioned later, most such lines are now believed to be composite, consisting of both emission and absorption. It will be noted that there are very few of the stellar lines for which there is a single unambiguous identification, the majority being blends of several components.

Equivalent Widths

The plates on which the stellar spectrograms were made were all calibrated with the aid of a rapidly rotating step sector (100 r.p.s.) placed in front of the slit of a calibrating spectrograph.

For the measurements of intensity the microphotometer tracings were transformed into true graphs of intensity with the aid of the Victoria intensitometer, which has been previously described (5). The equivalent widths of the lines were determined with the aid of a planimeter, the results being expressed both in angstrom units and in displacement in kilometers per second. Since the spectrum is known to be variable, a complete treatment of the subject of line intensities would involve separate values for each date. Actually

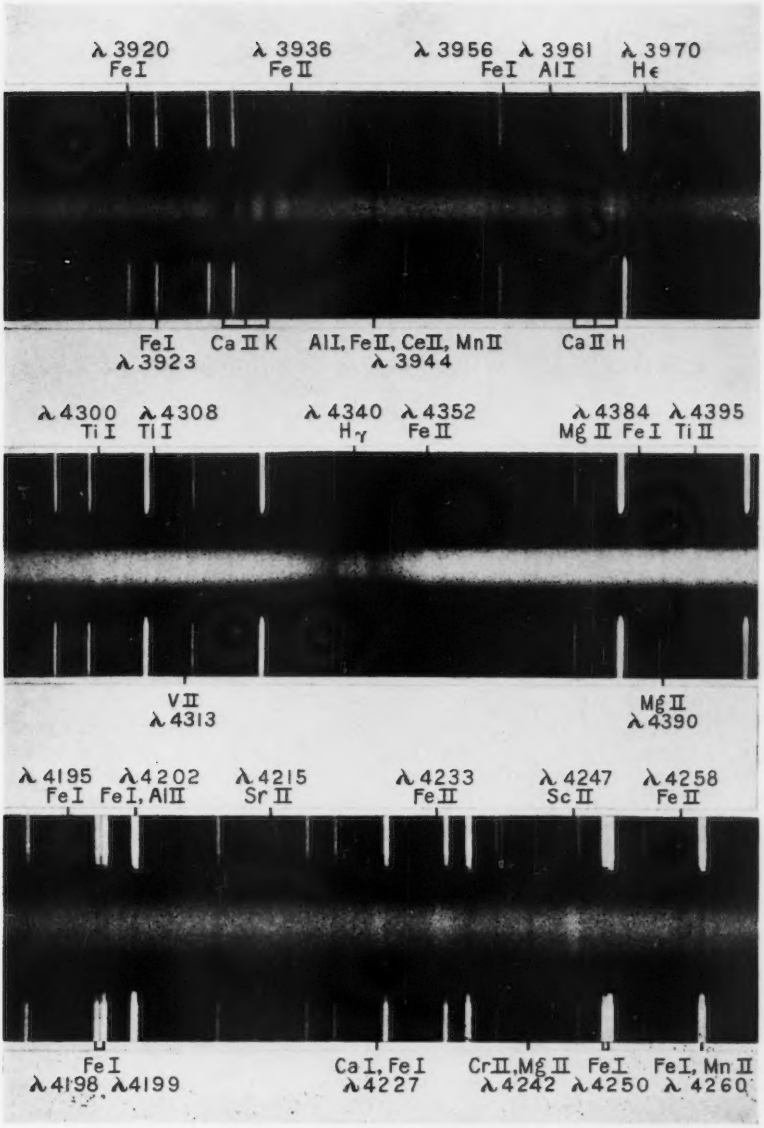

Spectra of H.D. 190073.

The two upper sections of the spectrum are from the II M plate. The lower one is of II L dispersion.

Micrometer machine for measurement of tracings. In the machine may be seen a tracing of the line λ 3968 of CaII with accompanying iron comparison spectrum.

in most cases the variations are small and it is considered that a table of mean values of intensity is the only practicable way of treating the data at the present time.

In view of the complex character of most of the emission lines, it is necessary to consider a number of the actual profiles in order to make clear the significance of the values given in the table. This has been done in Figs. 1 to 4 in which a variety of different types of profiles are shown. It is necessary to mention that no correction has been made for the distortions produced by the finite resolving power of the spectrograph.

For profiles where the absorption and emission components are clearly separated there is little ambiguity as to the significance of the values of equivalent width given in Table II. Even for the very complex lines of CaII the two displaced absorption components are well separated, and while there is undoubtedly some overlapping the general indication of intensity given by the integration of the area under the continuous spectrum is quite clear. A considerable number of the emission lines of this star, however, have absorption components directly superimposed upon the emission, as for example the FeII line λ 4233 of Fig. 1. The number of lines exhibiting these characteristics is very much greater on spectrograms of high dispersion. Many wave lengths that appeared to be pure absorption or pure emission when observed with single-prism dispersion are clearly a combination of the two when seen on two-prism plates. In particular, it is interesting to record that the lines of FeI which were first thought to be pure absorption are now definitely seen to have weak emission wings as shown in Fig. 1. It seems quite possible in fact that all the lines in the spectrum if observed with sufficient dispersion and contrast would display a composite character.

Profiles of the general character of the complex lines of Fig. 1 are sufficiently indicated in Table II by the fact that the same wave length is associated with both absorption and emission components. In this connection, the wave lengths λ3933.70 CaII, λ4045.78 FeI, and λ4233.23 FeII may be quoted. The tabular value of equivalent width for the absorption is obtained by integrating the area included between the reconstructed emission profile and the line indicating the absorption, the result being divided by the mean ordinate of the top of the emission profile to reduce it to the continuous spectrum (See Fig. 1). The emission intensity is derived by simply integrating the area of the reconstructed emission profile. It should be clearly understood that equivalent widths derived in this way are of limited application and serve only as a general indication of the relative intensity of line components. Complete line profiles will be required for a detailed discussion of the interpretation of the observations.

Numerical Data

Table II, in which all numerical data are listed, consists of nine columns as follows. Column 1 contains the adopted wave lengths in angstroms of all lines measured in the spectrum. In Columns 2 and 3 the wave lengths as

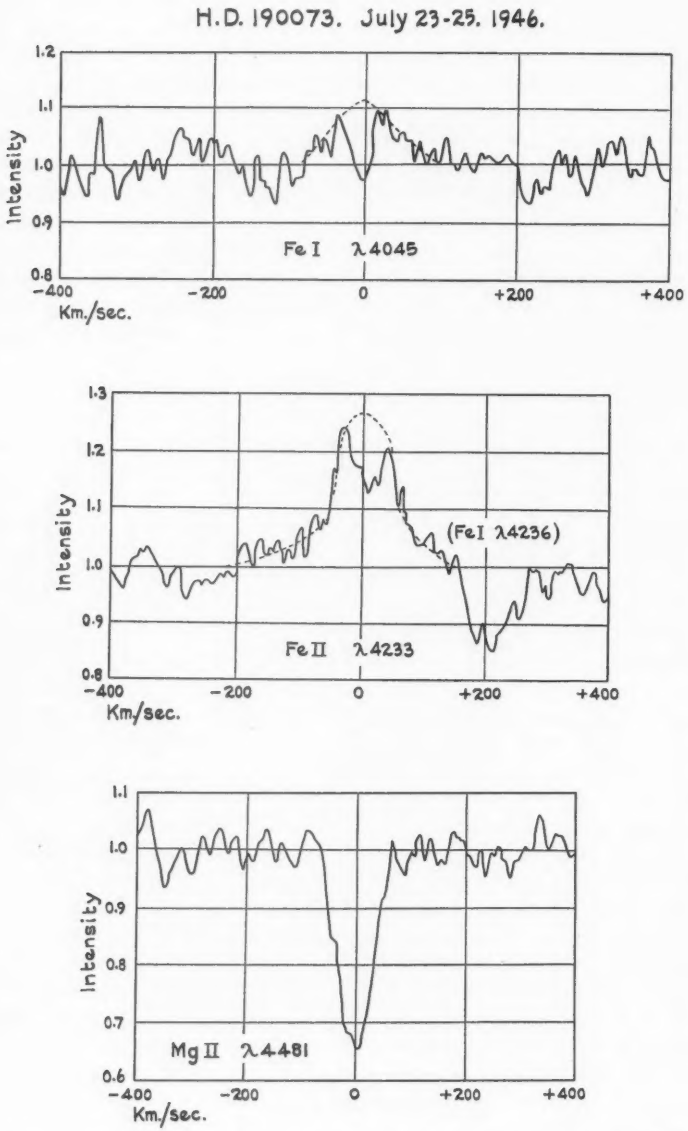

FIG. 1. *Intensity profiles of lines in the spectrum of H.D. 190073. Dispersions as follows:* λ *4045, 8.0* Å *per mm.;* λ *4233, 10.0* Å *per mm.;* λ *4481, 13.0* Å *per mm.*

derived from one and two-prism plates are compared. Column 4 gives the type of the line, A indicating absorption and E, emission. Columns 5 and 6 give the equivalent width first in angstrom units and then in velocity units of kilometers per second. The last three columns, Nos. 7, 8, and 9, are concerned with identification and give, respectively, the laboratory wave length of the line, the observed laboratory intensity, and the atom with which it is associated. In a few instances where the line has not been observed in the laboratory the symbol ⊙ indicates that it has been observed in the solar spectrum.

TABLE II

WAVE LENGTHS, INTENSITIES, AND IDENTIFICATIONS OF LINES IN THE SPECTRUM OF H.D. 190073

Adopted wave length	Wave length, 1-prism	Wave length, 2-prism	Type	E.W., Å	E.W., km./sec.	Identification		
3849.90	49.90	—	A	0.09	7.2	3849.97	(40)	FeI
						49.76	(3)	VII
3853.88	53.88	—	A	0.07	5.3	3853.72	(10n)	TiI
3856.10	56.10	—	A	0.17	12.9	3856.07	(3)	NII
						56.16	(1)	AII
						56.02	(8)	SiII
3862.59	62.59	—	A	0.10	7.5	3862.59	(6)	SiII
3863.92	63.92	—	A	0.05	3.9	3863.95	(1)	FeII
3865.36	65.36	—	A	0.10	7.9	3865.53	(30)	FeI
3867.04	67.04	—	A	0.07	5.7	3867.22	(7)	FeI
3872.63	72.63	—	A	0.09	7.1	3872.62	(60)	GdII?
						72.50	(60)	FeI
3877.77	77.77	—	A	0.15	11.5	3877.59	(2n)	TiI
						78.02	(60)	FeI
3878.38	78.38	—	A	—	—	3878.58	(100r)	FeI
3896.60	—	96.60	A	—	—	3896.53	(10)	ZrI
3900.76	00.76	—	E	0.29	22.0	3900.51	(10)	ZrI
3903.00	02.92	03.04	A	0.07	5.7	3902.92	(50)	CrI
						02.95	(20)	FeI
3905.63	05.65	05.62	A	0.15	11.8	3905.66		FeI**
						05.64	(25)	CrII
						05.53	(100)	SiI
3906.53	06.53	—	A	—	—	3906.48	(8)	FeI
3912.92	12.85	12.96	E	0.07	5.6	3912.89	(4)	VI
						12.98	(5)	NiI
3913.47	—	13.47	A	0.04	3.3	3913.46	(60)	TiII

** *Predicted.*

TABLE II—*Continued*

WAVE LENGTHS, INTENSITIES, AND IDENTIFICATIONS OF LINES IN THE SPECTRUM OF H.D. 190073—*Continued*

Adopted wave length	Wave length, 1-prism	Wave length, 2-prism	Type	E.W., Å	E.W., km./sec.	Identification		
3913.89	13.82	13.93	E	0.06	4.4	3913.64	(4)	FeI
3914.44	—	14.44	A	0.06	4.7	3914.48	(2)	FeII
3916.41	16.21	16.51	A	0.08	6.0	3916.24	(25)	CrI
						16.48	(200)	TmI
3918.56	18.60	18.53	A	0.07	5.3	3918.64	(6)	FeI
						18.58	(⊙)	FeI
3920.20	20.16	20.22	A	0.04	3.4	3920.26	(20r)	FeI
3922.94	22.88	22.96	A	0.05	4.0	3922.91	(25R)	FeI
3926.04	—	26.04	A	0.04	3.2	3925.95	(6)	FeI
3927.94	—	27.94	A	0.06	4.8	3927.92	(30R)	FeI
3929.41	29.36	29.43	A	1.22	93.4	3933.66		CaII*K
3931.36	31.29	31.38	A	0 73	56.0	3933.66		CaII*K
3933.70	33.63	33.72	E	1.11	84.6	3933.66	(400R)	CaII K
			A	0.93	70.6			
3935.96	35.99	35.95	A	0.07	5.2	3935.94	(6)	FeII
						35.96	(30)	CoI
3938.32	38.40	38.28	A	0.07	5.2	3938.29	(2)	FeII
						38.40	(0)	MgI
3944.02	43.97	44.03	A	0.09	7.0	3944.01	(10R)	AlI
						43.83		FeII
						43.89	(100)	CeII
						43.86		MnII
3945.29	45.16	45.32	A	0.03	2.0	3945.12	(4)	FeI
						45.21		FeII**
						45.33	(15)	CoI
						45.50	(9)	CrI
3947.52	47.76	47.39	A	0.06	4.5	3947.39	(1)	FeI
						47.77	(40)	TiI
						47.30	(10)	OI
3955.62	—	55.62	A	0.01	1.0	3955.77	(⊙)	FeI
3956.72	56.63	56.76	A	0.11	8.1	3956.68	(12)	FeI
						56.46	(9)	FeI
3961.63	—	61.63	A	0.05	3.8	3961.52	(10R)	AlI
3964.29	64.16	64.33	A	0.84	63.6	3968.47		CaII*H
3966.17	66.11	66.18	A	0.47	35.7	3968.47		CaII*H

* *Displaced calcium line.*
** *Predicted.*

TABLE II—*Continued*

WAVE LENGTHS, INTENSITIES, AND IDENTIFICATIONS OF LINES IN THE SPECTRUM OF H.D. 190073—*Continued*

Adopted wave length	Wave length, 1-prism	Wave length, 2-prism	Type	E.W., Å	E.W., km./sec.	Identification		
3968.56	68.55	68.56	E A	1.06 0.58	80.4 44.0	3968.47	(350R)	CaII H
			A	10.37	782.7	3970.07		$H\epsilon$†
3981.95	82.31	81.77	A	0.04	2.8	3981.78 82.48	(7) (30)	FeI TiI
3984.00	83.89	84.03	A	0.05	4.0	3983.96 83.83 83.91	(10) (⊙) (100)	FeI FeI CrI
3986.63	86.45	86.68	A	0.04	3.1	3986.40	(2)	MnI
3987.32	87.32	—	A	0.05	3.8	3987.46	(2)	MnI
3997.42	97.30	97.48	A	0.06	4.6	3997.39	(15)	FeI
3998.06		98.06	A	0.03	2.2	3998.05	(10)	FeI
4002.40	02.48	02.35	A	0.07	5.4	4002.66 02.55 02.47	(1) (3) (9n)	FeI FeII TiI
4003.02		03.02	A	0.05	3.9	4003.33	(25)	CrII
4005.18	05.24	05.14	A	0.06	4.4	4005.25	(25)	FeI
4005.86	—	05.86	A	0.04	2.8	4005.71	(800)	VII
4012.45	12.42	12.45	A	0.10	7.1	4012.49 12.47	(20) (1)	CrI FeII
4014.55	14.48	14.57	A	0.04	3.2	4014.53 14.67 14.49	(10) (10) (5)	FeI CrI ScII
4015.51	—	15.51	A	0.02	1.8	4015.50	(1)	NiII
4017.25	17.25	—	A	0.03	2.5	4017.27 17.29	(1) (15n)	CII VII
4021.94	—	21.94	A	0.04	2.8	4021.87	(12)	FeI
4023.37	23.26	23.40	A	0.03	1.9	4023.39	(600)	VII
4024.60	24.78	24.56	A	0.07	5.1	4024.55 24.74	(5) (6n)	FeII FeI
4025.14	—	25.14	A	0.04	2.8	4025.14 25.11	(2) (3)	TiII NiI
4028.34	28.29	28.35	A	0.05	4.0	4028.33	(7)	TiII

† *Broad underlying hydrogen line.*

TABLE II—*Continued*

WAVE LENGTHS, INTENSITIES, AND IDENTIFICATIONS OF LINES IN THE SPECTRUM OF H.D. 190073—*Continued*

Adopted wave length	Wave length, 1-prism	Wave length, 2-prism	Type	E.W., Å	E.W., km./sec.	Identification		
4029.64	—	29.64	A	0.03	2.1	4029.64	(P)	TiII
						29.64	(3n)	FeI
4030.62	30.68	30.60	A	0.07	4.9	4030.76	(200R)	MnI
						30.50	(6)	FeI
						30.51	(25n)	TiI
4032.96	32.88	32.98	A	0.05	4.0	4033.07	(150R)	MnI
						32.95	(3)	FeII
4034.52	—	34.52	A	0.04	3.2	4034 49	(100R)	MnI
4035.67	35.63	35.68	A	0.05	3.9	4035.63	(400)	VII
						35.54	(8)	CoI
						35.73	(15)	MnI
4044.11	44.11	—	A	0 03	1.9	4044.14	(8R)	KI
4045.78	46.04	45.72	E	0.12	8.6	4045.82	(60r)	FeI
			A	0.06	4.6	46.07	(⊙)	FeI
						46.19	(3)	CrI
4048.87	48.97	48.84	A	0.05	4.0	4048.83	(3)	FeII
						48.76	(15)	MnI
4051.96	52.07	51.93	A	0.05	3.4	4051.92	(2)	FeI
						51.97	(12)	CrII
4053.88	53.95	53.86	A	0.08	6.1	4053.82	(1)	FeI
						53.81	(3)	TiII
4057.47	57.40	57.48	A	0.06	4.4	4057.36	(2)	FeI
						57.35	(2)	NiI
						57.50	(5n)	MgI
4060.14	—	60.14	A	0.01	1.0	4060.26	(20)	TiI
4062.01	61.69	62.17	A	0.02	1.3	4061.79	(1)	FeII
						61.77		CrII
						62.22	(60)	CeII
4063.53	63.44	63.55	E	0.06	4.6	4063.60	(45)	FeI
			A	0.06	4.8			
4064.50	—	64.50	A	0.01	0.9	4064.35	(1)	TiII
						64.58	(300)	SmII
4065.06	—	65.06	A	0.04	2.7	4065.07	(100)	VII
4067.01	67.14	66.98	A	0.07	5.0	4066.98	(6)	FeI
						67.05	(3)	NiII
						67.28	(4)	FeI
4067.98	—	67.98	A	0.03	1.9	4067.98	(8n)	FeI
4070.80	—	70.80	A	0.04	3.0	4070.77	(5n)	FeI

TABLE II—*Continued*

WAVE LENGTHS, INTENSITIES, AND IDENTIFICATIONS OF LINES IN THE SPECTRUM OF H.D. 190073—*Continued*

Adopted wave length	Wave length, 1-prism	Wave length, 2-prism	Type	E.W., Å	E.W., km./sec.	Identification		
4071.77	71.68	71.82	E A	0.08 0.06	5.6 4.4	4071.74 71.54	(40) (8)	FeI VI
4073.62	—	73.62	A	0.01	1.0	4073.76 73.76	(4n) (1500)	FeI GdII
4076.62	76.56	76.64	A	0.05	3.4	4076.64 76.50	(8n) (1)	FeI FeI
4077.73	—	77.73	A	0.03	2.4	4077.71	(400r)	SrII
4083.61	—	83.61	A	0.02	1.4	4083.55 83.58	(1) (100)	FeI SmII
4101.93	01.99	01.92	E A	0.52 0.17	37.9 12.7	4101.74		H_δ*
			A	12.50	913.2	4101.74		H_δ†
4110.41	—	10.41	A	0.03	2.3	4110.38	(60)	CeII
4118.62	—	18.62	A	0.05	3.4	4118.55	(15)	FeI
4122.65	22.55	22.67	A	0.05	3.7	4122.64 22.52	(4) (4)	FeII FeI
4128.08	28.11	28.07	A	0.16	11.4	4128.05	(8)	SiII
4130.93	30.90	30.94	A	0.14	9.8	4130.88	(10)	SiII
4132.12	32.11	32.12	A	0.09	6.2	4132.06 32.16	(25) (4)	FeI CoI
4134.63	34.57	34.64	A	0.04	3.0	4134.68 34.72	(12) (30)	FeI KII
4136.69	36.80	36.63	A	0.04	2.6	4136.51	(1)	FeI
4143.67	43.58	43.69	A	0.08	5.9	4143.42 43.87 43.76	(15) (30) (2)	FeI FeI HeI
4145.86	—	45.86	A	0.04	3.2	4145.77	(25)	CrII
4147.18	—	47.18	A	0.03	2.1	4147.34	(⊙)	FeI
4149.27	—	49.27	E A	0.13 0.07	9.4 5.2	4149.37	(5n)	FeI
4153.95	54.19	53.89	A	0.07	5.0	4153.82 53.91	(25) (10n)	CrI FeI
4154.75	—	54.75	A	0.07	4.9	4154.50 54.86	(12) (2)	FeI TiI

* *Emission component of hydrogen line.*

† *Broad underlying hydrogen line.*

TABLE II—*Continued*

WAVE LENGTHS, INTENSITIES, AND IDENTIFICATIONS OF LINES IN THE SPECTRUM OF H.D. 190073—*Continued*

Adopted wave length	Wave length, 1-prism	Wave length, 2-prism	Type	E.W., Å	E.W., km./sec.	Identification		
4156.81	—	56.81	E A	0.08 0.07	5.8 5.0	4156.80	(12)	FeI
4161.66	—	61.66	A	0.03	1.9	4161.80	(30)	SrII
4163.65	—	63.65	E A	0.12 0.06	8.9 4.6	4163.64 63.68	(40) (1)	TiII FeI
4167.30	67.28	67.30	A	0.08	5.4	4167.26 67.27	(10n) (10n)	MgI MgI
4171.94	71.99	71.92	A	0.05	3.8	4171.90 71.90	(30) (2)	TiII FeI
4173.48	—	73.48	E A	0.07 0.06	4.7 4.2	4173.45	(8)	FeII
4175.55	—	75.55	A	0.06	4.2	4175.64	(10)	FeI
4176.58	—	76.58	A	0.02	1.4	4176.57	(7n)	FeI
4177.75	—	77.75	E A	0.16 0.07	11.5 5.1	4177.70		FeII
4178.85	—	78.85	A	0.02	1.2	4178.86	(8)	FeII
4181.83	—	81.83	A	0.03	2.5	4181.76	(15)	FeI
4184.35	84.01	84.51	A	0.06	4.4	4184.22	(1)	FeI
4186.16	—	86.16	A	0.02	1.4	4186.12 86.24	(25) (30)	TiI KII
4187.19	87.40	87.19	A	0.04	3.2	4187.04 87.25	(20) (4)	FeI CoI
4187.86		87.86	A A	0.07 0.06	5.2 4.4	4187.80	(20)	FeI
4191.21	91.33	91.21	A	0.03	1.8	4191.27	(25)	CrI
4191.57		91.57	A A	0.04 0.04	2.8 2.6	4191.44 91.56	(15) (10)	FeI VI
4195.58	—	95.58	A	0.03	2.4	4195.62	(3)	FeI
4196.96	—	96.96	E A	0.03 0.01	2.4 1.0	4197.10	(⊙)	FeI
4198.33	98.61	98.33	A	0.07	5.0	4198.31	(20)	FeI
4199.15		99.15	A A	0.10 0.07	7.4 5.3	4199.10	(20)	FeI
4200.65	—	00.65	E A	0.10 0.07	7.1 4.8	4200.75	(6)	TiI
4202.01	01.99	02.02	A	0.08	5.5	4202.03 02.40	(30) (2)	FeI Al II

TABLE II—*Continued*

WAVE LENGTHS, INTENSITIES, AND IDENTIFICATIONS OF LINES IN THE SPECTRUM OF H.D. 190073—*Continued*

Adopted wave length	Wave length, 1-prism	Wave length, 2-prism	Type	E.W., Å	E.W., km./sec.	Identification
4209.79	—	09.79	A	0.07	5.2	4209.76 (15) CrI 09.86 (20) VI
4210.41	—	10.41	A	0.08	5.6	4210.35 (15) FeI
4215.58	—	15.58	A	0.04	2.8	4215.52 (300r) SrII
4216.60	—	16.60	E	0.05	3.7	
4219.41	19.40	19.41	A	0.04	2.6	4219.51 (2) VI 19.36 (12) FeI
4221.09	—	21.09	E	0.02	1.4	
4222.24	—	22.24	A	0.04	2.7	4222.22 (12) FeI
4223.08	—	23.08	A	0.01	0.9	4223.04 (5) NI
4224.82	24.73	24.87	A	0.05	3.4	4224.85 (20) CrII 24.80 (5) TiI
4226.53	26.52	26.53	E A	0.11 0.02	8.1 1.4	4226.73 (500R) CaI 26.43 (3) FeI
4227.31	—	27.31	A	0.02	1.4	4227.43 (30) FeI
4228.26	—	28.26	E A	0.02 0.02	1.3 1.2	
4233.23	33.25	33.23	E A	0.48 0.06	34.3 4.2	4233.17 (11) FeII 33.25 (10) CrII
4235.93	35.77	35.97	A	0.10	7.1	4235.94 (25) FeI
4238.85	—	38.85	A	0.06	4.4	4238.82 (10n) FeI 38.96 (35) CrI
4242.46	—	42.46	A	0.06	4.5	4242.38 (30) CrII 42.47 (4) MgII
4246.92	47.01	46.90	E A	0.33 0.04	23.0 2.5	4246.83 (100) ScII
4250.17	50.35	50.17	A	0.06	4.4	4250.12 (25) FeI
			A	0.06	4.3	
4250.80		50.80	A	0.05	3.7	4250.79 (25) FeI
4251.77	—	51.77	E	0.02	1.6	4251.77 (2n) TiI
4252.68	—	52.68	A	0.05	3.2	4252.62 (10) CrII
4254.39	—	54.39	A	0.02	1.2	4254.35 (1000R) CrI
4256.23	—	56.23	A	0.02	1.4	4256.21 (3) FeI
4258.13	—	58.13	A	0.12	8.4	4258.16 (3) FeII

TABLE II—*Continued*

WAVE LENGTHS, INTENSITIES, AND IDENTIFICATIONS OF LINES IN THE SPECTRUM OF H.D. 190073—*Continued*

Adopted wave length	Wave length, 1-prism	Wave length, 2-prism	Type	E.W., Å	E.W., km./sec.	Identification		
4260.46	60.40	60.47	A	0.09	6.6	4260.48 60.47	(35)	FeI MnII**
4261.24	—	61.24	E	0.02	1.2	4261.35	(25)	CrI
4261.92	61.93	61.92	A	0.05	3.8	4261.92	(20)	CrII
4271.58	71.52	71.60	A	0.09	6.1	4271.65 71.55	(⊙) (12)	FeI VI
4273.32	—	73.32	A	0.03	2.0	4273.32 73.31	(3) (2)	FeII TiI
4275.53	—	75.53	A	0.04	2.9	4275.57	(30)	CrII
4282.25	—	82.25	A	0.05	3.6	4282.41	(12)	FeI
4284.20	—	84.20	A	0.05	3.8	4284.21	(20)	CrII
4287.96	—	87.96	A	0.05	3.6	4287.89	(2)	TiII
4290.75	—	90.75	E	0.12	8.6			
4292.36	92.23	92.42	E A	0.17 0.08	12.0 5.7	4292.29	(1)	FeI
4294.15	—	94.15	E A	0.17 0.07	12.2 5.2	4294.10	(40)	TiII
4296.52	—	96.52	A	0.06	4.2	4296.57	(6)	FeII
4297.85	—	97.85	A	0.04	2.6	4297.74	(30)	CrI
4299.13	98.80	99.21	A	0.06	4.2	4298.66 99.23	(40) (15)	TiI TiI
4299.71		99.71	E	—	—	4300.05 299.72	(60) (20)	TiII CrI
4300.53	00.55	00.53	E A	0.25 0.06	17.7 4.3	4300.57	(50)	TiI
4303.78	03.77	03.78	E	0.05	3.7			
4305.61	05.49	05.64	A	0.04	2.9	4305.46 05.72	(3) (10)	FeI ScII
4306.23	—	06.23	E	0.03	2.4			
4307.32	—	07.32	E	0.03	2.4			
4307.84	—	07.84	E A	0.22 0.11	15.2 7.4	4307.90 07.91	(40) (35)	TiII FeI
4308.53	—	08.53	E	0.07	5.0	4308.51	(2)	TiI
4313.55	—	13.55	E	0.05	3.2	4313.30	(2)	VII

** *Predicted.*

TABLE II—*Continued*

WAVE LENGTHS, INTENSITIES, AND IDENTIFICATIONS OF LINES IN THE SPECTRUM OF H.D. 190073—*Continued*

Adopted wave length	Wave length, 1-prism	Wave length, 2-prism	Type	E.W., Å	E.W., km./sec.	Identification		
4314.19	—	14.19	A	0.03	2.0	4314.08 14.29	(60) (4)	ScII FeII
4315.14	—	15.14	A	0.01	0.7	4315.09	(10)	FeI
4316.84	—	16.84	A	0.03	2.1	4316.81	(1)	TiII
4319.98	—	19.98	E A	0.02 0.02	1.6 1.5	4320.36	(1)	FeI
4320.98	—	20.98	A	0.05	3.3	4320.74 20.96	(50) (1)	ScII TiII
4336.75	—	36.75	A	0.09	6.5	4340.47		H_γ*
4338.86	—	38.86	A	0.26	17.9	4340.47		H_γ*
4340.58	—	40.58	E A	1.73 0.32	119.8 22.2	4340.47		H_γ†
			A	13.39	924.7	4340.47		H_γ‡
4351.84	51.74	51.86	E A	0.34 0.04	23.1 2.9	4351.76	(9)	FeII
4357.48	—	57.48	A	0.03	2.0	4357.57 57.52	(4) (15)	FeII CrI
4367.90	68.01	67.90	A	0.08	5.8	4367.91	(2)	FeI
			A	0.06**	4.4**			
4369.66		69.66	A	0.08	5.6	4369.61 69.68	(5n)	FeII TiI
4375.32	—	75.32	E	0.07	4.9	4375.33	(30)	CrI
4384.62	—	84.62	E A	0.42 0.16	28.5 10.8	4384.64 84.13	(8) (⊙?)	MgII FeI
4386.01	85.92	86.06	E	0.06	4.2			
4386.90	—	86.90	E A	0.63 0.07	43.3 5.1	4386.86	(10)	TiII
4388.93	—	88.93	A	0.18	12.1	4389.12		VII
4390.71	90.66	90.72	A	0.14	9.4	4390.58	(10)	MgII
4394.69	94.86	94.69	E					
4395.20		95.29	E A	0.38 0.08	25.7 5.6	4395.03	(60)	TiII
4404.81	—	04.81	E A	0.15 0.06	10.2 4.2	4404.75	(30)	FeI

* *Displaced hydrogen line.*

† *Emission component of hydrogen line.*

‡ *Broad underlying hydrogen line.*

** *Single prism observations.*

TABLE II—*Continued*

WAVE LENGTHS, INTENSITIES, AND IDENTIFICATIONS OF LINES IN THE SPECTRUM OF H.D. 190073—*Continued*

Adopted wave length	Wave length, 1-prism	Wave length, 2-prism	Type	E.W., Å	E.W., km./sec.	Identification		
4415.31	—	15.31	A	0.06	4.3	4415.12	(20)	FeI
4416.40	16.66	16.27	E	0.10	6.8			
4422.08	—	22.08	A	0.05	3.7	4421.95	(1)	TiII
4434.02	—	34.02	A	0.09	6.4	4433.99	(8)	MgII
4443.40		43.40	E					
4443.92	43.87	43.93	E A	0.33 0.04	22.2 2.4	4443.80	(50)	TiII
4455.02	54.67	55.19	A	0.07	4.6	4455.26 54.78	(3) (80)	FeII CaI
4468.69	68.60	68.71	E A	0.43 0.05	28.9 3.5	4468.49	(50)	TiII
4476.20	—	76.20	A	0.03	2.2	4476.08	(4)	FeI
4481.36	81.26	81.38	A	0.42	27.9	4481.33 81.13	(100) (100)	MgII MgII
4488.05	88.05	—	A	0.08	5.1	4488.05	(30)	CrI
4501.55	01.33	01.61	E	0.38	25.4	4501.27	(40)	TiII
4508.62	08.27	08.70	E	0.24	16.1	4508.28	(8)	FeII
4515.55	15.58	15.53	E	0.18	12.0	4515.34	(7)	FeII
4522.52	22.37	22.56	E A	0.45 0.06	30.0 3.9	4522.63	(9)	FeII
4534.13	33.57	34.27	E A	0.26 0.04	17.3 2.8	4534.17	(2)	FeII
4549.95	49.83	49.98	E A	0.54 0.10	35.3 6.8	4549.62	(60n)	TiII
4556.29	55.45	56.71	E	0.31	20.7	4556.76	(4)	VII
4559.36	—	59.36	E	0.11	7.4			
4564.10	63.65	64.21	E	0.21	14.0	4563.76	(30)	TiII
4572.29	72.24	72.31	E A	0.44 0.06	28.7 3.7	4571.97	(50n)	TiII
4584.21	83.84	84.30	E A	0.65 0.15	42.4 10.0	4583.83	(11)	FeII
4703.01	03.01	—	A	—	—	4702.98 02.98 02.99	 (40)	MgI MgI MgI

TABLE II—*Concluded*

WAVE LENGTHS, INTENSITIES, AND IDENTIFICATIONS OF LINES IN THE SPECTRUM OF H.D. 190073—*Concluded*

Adopted wave length	Wave length, 1-prism	Wave length, 2-prism	Type	E.W., Å	E.W., km./sec.	Identification		
4857.27	57.27	—	A	0.14	8.7	4861.33		H_β*
4860.75	60.75	—	E	3.09	190.5	4861.33		H_β†
			A	10.44	644.0	4861.33		H_β‡
4920.08	20.08	—	A	0.12	7.1			
4923.79	23.79	—	E A	1.14 0.18	69.3 11.0	4923.92	(12)	FeII

* *Displaced hydrogen line.*

† *Emission component of hydrogen line.*

‡ *Broad underlying hydrogen line.*

Line Profiles

The increased resolving power afforded by two prisms has revealed additional detail in the line profiles and has made it possible to clarify a number of points that were formerly uncertain. One such matter concerns the relative intensities of the central reversals appearing in the emission components of the H and K lines of CaII. Struve and Swings (8), on the basis of relatively low dispersion, had suggested that the central reversal of the H line was abnormally weak relative to that of K and indeed there seemed some doubt as to whether the H absorption was present at all on their plates. From this they concluded that the reversal at H was affected by the broad hydrogen absorption and therefore arose in a low level in the stellar atmosphere.

Profiles of both the H and K lines of calcium from the two-prism plates are shown in Fig. 2. From this illustration it will be seen that the absorption in the normal position of CaII H is relatively conspicuous. It is difficult to arrive at a reliable estimate of the intensity of the line since this depends upon assumptions as to the form of the undistorted emission. However, on the basis of the reconstruction shown by the broken lines of Fig. 2, the equivalent widths of K and H are 71 km. per sec. and 44 km. per sec., while the central intensities are 0.29 and 0.50 respectively, with excellent agreement between the two high-dispersion plates. It would thus appear that these absorption features for H and K stand in normal relationship to one another and the intensity data are not inconsistent with an origin of this absorption in the outer envelope of the star.

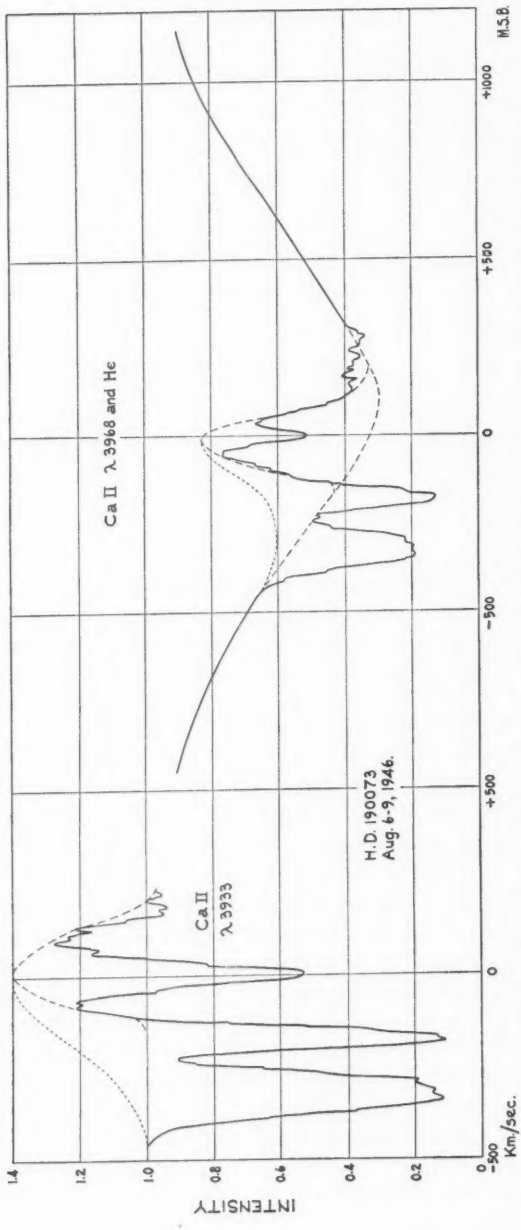

FIG. 2. *Profiles of CaII lines. The dotted lines correspond to alternative suggestions for reconstructing the undistorted emission.*

An interesting aspect of the CaII lines is the fact that the more displaced component of the two P Cygni absorption features is approximately twice the width of its companion. The structure shown in the bottom of the wider component appears to be real and it would be interesting to see whether it is variable. Unfortunately one of our high-dispersion plates was too weak to record detail in the bottom of this very strong line. The additional structure shown on the violet emission wing of the H line of calcium as well as the unsymmetrical character of this line is possibly a consequence of blending with the weak P Cygni line of hydrogen which is superimposed on the broad H_ϵ absorption.

It will be further noted that the maximum between the two strong displaced absorption lines approaches very close to the continuous spectrum for K and the wing of the hydrogen profile for H. The question thus arises as to whether, if still higher dispersion were used, this maximum might not have a central intensity greater than that of the continuous spectrum. This consideration, together with others already advanced in connection with a suggested explanation of the hydrogen line profiles of the star M.W.C. 374 (4), raises the question as to whether a quite different reconstruction of the emission profile than that shown by the heavy dotted lines in Fig. 2 may not give a clearer picture of the emitting envelope. In view of the great strength of the displaced absorption lines, it seems reasonable to suppose that the envelope emits in these wave lengths also and that the emission may have been suppressed by strong absorption. If this is the case, then the reconstructed emission profile would be markedly unsymmetrical as shown by the fine dotted lines of Fig. 2. Such asymmetry could arise as a consequence of occultation by the star's disk of that part of the envelope having the largest velocity of recession, and if this is the correct explanation then the conclusion follows that the diameter of the emitting envelope does not greatly exceed that of the central star.

Similar considerations may apply in connection with the lines of hydrogen. Profiles of H_γ for the two high-dispersion plates are shown in Fig. 3. The difference in character between these two profiles clearly indicates the variable character of the spectrum. For the plate taken on July 23-25, 1946, there are two displaced absorption lines which are similar as regards displacement with the corresponding features of CaII although their relative intensities are quite different. On the plate of Aug. 6-9, 1946, only one displaced line definitely appears. Both profiles, however, exhibit a clearly marked asymmetry about the normal position, the extension to the violet being much greater than that to the red. Again, as for CaII, this appears most readily explicable in terms of occultation by the star's disk and again an envelope of relatively small dimensions is suggested.

Reference has already been made to the line profiles of FeI and FeII in connection with the discussion of equivalent widths. The central reversals shown by these and other lines represent possibly the most significant single feature of this remarkable spectrum. It is interesting to note that the metallic

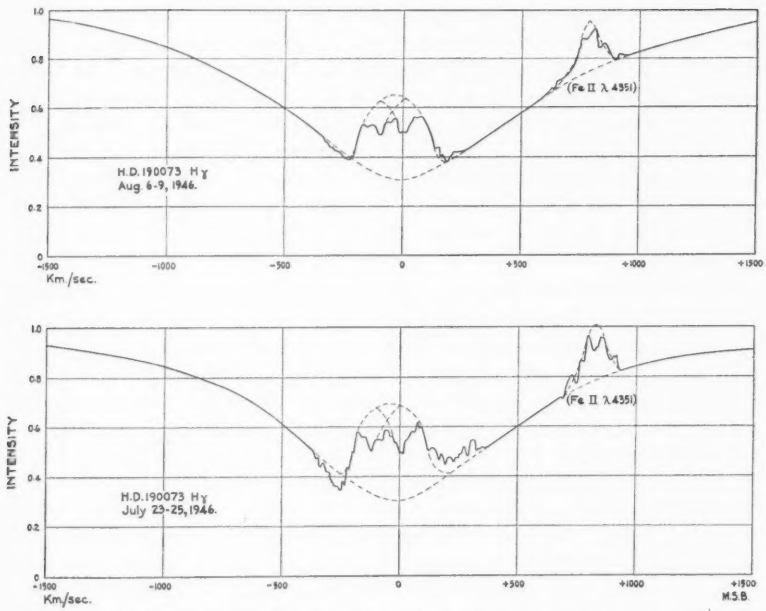

FIG. 3. *Profiles of H_γ on different dates. Of special interest is the unsymmetrical character of the emission profile and the evidence of variability in the spectrum.*

lines in the less refrangible region of the spectrum to the red of λ 4400 no longer show evidence of reversal and this is attributed to insufficient resolving power.

The profiles of the D lines of sodium are shown as pure emission lines in Fig. 4 as observed with three-prism dispersion of 34.5 Å per mm. It would

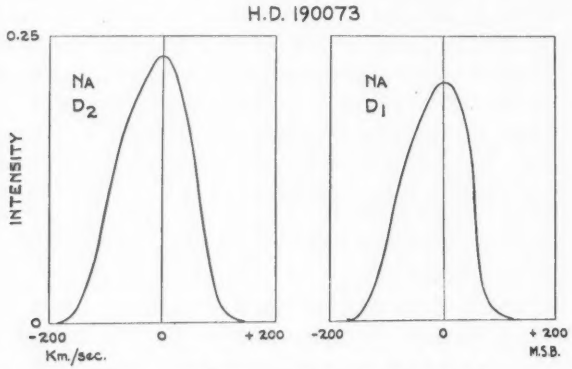

FIG. 4. *Sodium emission line profiles. The dispersion of 34.5 Å per mm. is insufficient to indicate whether or not these profiles are of complex structure.*

be well worth while for any observatory with sufficiently powerful equipment to examine these lines with high dispersion (say 10 Å per mm.) to see whether they share the feature of central reversal with other metallic lines.

The only really strong line in the spectrum which shows no clear evidence of complexity on our plates is MgII λ 4481. A profile of this line is shown in Fig. 1 and it is seen to be a strong narrow absorption feature in no way differing in appearance from the same line in many normal stellar spectra. It is worth recording that there are several other emission line stars including H.D. 51480 and H.D. 45910 in which the MgII line also appears as pure absorption.

Conclusion

Apart from the addition of many new wave lengths and identifications to the known spectrum of H.D. 190073 the most important result of the present study is to be found in the clearer delineation of line profiles which makes possible a new approach to the question of interpretation.

The problem of the relative size of shell and envelope for an emission line star is a difficult one and in relatively few cases is a definitive answer possible. For the line H_γ in both high-dispersion plates the asymmetrical character of the emission profile appears to be beyond question and its interpretation in terms of an envelope of small size reasonably probable. The writers believe that this evidence supersedes the previous suggestion by Beals (2, 3) that the central absorption takes place in an envelope many times the diameter of the star and the criticism of this earlier interpretation by Struve and Swings (8) must now be regarded as valid.

While uncertainty still exists as to the part of the stellar envelope where the central absorption originates, absorption data on the H and K calcium line profiles are no longer inconsistent with an origin in the outer layers of the envelope. In this connection, it may be noted that evidence of strong absorption appears in the relatively intense hydrogen emission lines H_β and H_α (3), and it is clearly easier to attribute minima in such strong emission lines to absorption in an outer layer than in a layer deep in the star's atmosphere.

From the point of view of interpretation the most difficult feature of the spectrum is still the peculiar nature of the profiles associated with CaII. It was at first thought that the form of these lines was unique among stellar spectra but recent investigations have shown that this is not the case. The data of this paper indicate that the lines of hydrogen in H.D. 190073 show similar characteristics although the relative intensities of components are quite different. Double, displaced absorption has been observed on a number of occasions in the hydrogen lines of H.D. 45910 as well as other stars. Such profiles are, however, always of a variable character such as could be associated with temporary detached shells.

No great theoretical difficulty attaches to the explanation of such complex lines if it be assumed that they are associated with temporary nova-like shells. Among observed novae many complexities of this type are known and have

been explained on the basis of separate absorbing and emitting media moving independently of one another. For a permanent envelope the explanation is more difficult. A formal interpretation in terms of acceleration and subsequent deceleration of atoms within the envelope under conditions of dynamical equilibrium has been presented by Beals (2, 3). Such an explanation has considerable flexibility in accounting for the observed phenomena but so far the physical mechanism producing the accelerations is obscure. Whether the relatively complicated shell structure postulated by a theory of this general character can be shown to have a valid physical basis remains to be seen, but until some other explanation is forthcoming it would appear that the most promising line of approach to the problem of these complex line profiles is to be found in a study of the forces responsible for the radial motions of atoms ejected from the star.

References

1. Beals, C. S. Monthly Notices Roy. Astron. Soc. 96 : 730. 1936.
2. Beals, C. S. J. Roy. Astron. Soc. Can. 34 : 169. 1940.
3. Beals, C. S. J. Roy. Astron. Soc. Can. 36 : 145, 201. 1942.
4. Beals, C. S. J. Roy. Astron. Soc. Can. 37 : 241. 1943.
5. Beals, C. S. J. Roy. Astron. Soc. Can. 38 : 65. 1944.
6. Merrill, Paul W. Astrophys. J. 77 : 51. 1933.
7. Moore, Charlotte E. Contribs. Princeton Univ. Observ. No. 20. 1945.
8. Struve, Otto and Swings, P. Astrophys. J. 96 : 475. 1942.
9. Wyse, A. B. Lick Observ. Bull. No. 492, p. 129. 1938.

DESIGN OF GRID IONIZATION CHAMBERS[1]

By O. Bunemann,[2] T. E. Cranshaw,[3] and J. A. Harvey[4]

Abstract

Conformal representation theory is applied to a grid ionization chamber having plane parallel electrodes to give formulas useful in design. Expressions are obtained for the inefficiency of grid shielding of the electron collector, the spread of pulse size caused by the induced effect of positive ions, and the proportion of electrons collected by the grid. The theory was verified by experiment. The width of the polonium α-particle line at half-maximum was reduced to 50 kev. or about 1% of the energy by the use of a suitable grid and operating voltages. The corresponding standard deviation from all causes was 22 kev., made up of 2 kev. resulting from induced effect of positive ions, about 17 kev. from noise in the amplifier, and 14 kev. from straggling of ionization, thickness of source, and other effects. The spread caused by positive ions can therefore be almost completely eliminated by a grid.

Introduction

Many experimenters have used the number of ion pairs produced in the track of a charged particle in a gas filled ionization chamber to indicate the initial energy of the particle. The simplest chamber contains two plane parallel electrodes with an electrostatic field applied between them, that is, a high voltage electrode, and a collecting electrode that is connected to a suitable amplifier with a high resistance to ground. When an ionizing particle spends its energy in the gas between the electrodes the ions are collected and a pulse is fed to the amplifier. The rise time of this pulse depends on the orientation of the track in the chamber and the mobility of the components of the ionization, and its decay on the time constant of the capacity and leak resistance of the collecting electrode. This decay is usually arranged to be very long, and a short time constant later in the amplifier determines the output pulse duration. While this is frequently required to be short, the short time constant must be made about 10 times longer than the rise time. This condition is necessary to prevent the variation in rise time due to different track orientations from affecting the output pulse amplitude.

To permit the use of a fast amplifier by speeding up the rate of rise it is necessary first to use as a filling a gas that does not form negative ions by electron attachment, e.g., argon. The negative component of ionization then travels to the collector entirely as electrons, which have a high mobility. However the positive ions, which have a mobility less by a factor of about 1000,

[1] *Manuscript received May 28, 1949.*

Contribution from the Nuclear Physics and Theoretical Physics Branches, Division of Atomic Energy, National Research Council of Canada, Chalk River, Ontario. Issued as N.R.C. No. 1986. This work first appeared in Report CRP-247, dated May 1, 1946, of the National Research Council of Canada.

[2] *United Kingdom Staff; now at the Atomic Energy Research Establishment, Harwell, England.*

[3] *United Kingdom Staff; now at the Cavendish Laboratory, Cambridge University, Cambridge, England.*

[4] *Now at the Massachusetts Institute of Technology, Cambridge, Mass., U.S.A.*

induce a charge on the collector of the opposite sign. The potential of the collector will rise rapidly, as the electrons are collected, to an intermediate value given by the collected charge minus the induced charge divided by the capacity, and then rise slowly as the positive ions are removed, to the full potential. The induced charge depends on the orientation of the track in the chamber. If the induction effect of the positive ions can be eliminated the collector will attain its final potential immediately the electrons are collected.

The use of a grid to screen the electron-collecting electrode from the effect of the positive ions was suggested by O. R. Frisch (4). In such a three-electrode chamber the electron pulses are nearly proportional to the ionization in the tracks. The pulse consists of a rapid rise of the order of 1 μsec., and a fall determined as before. These fast pulses are more easily amplified linearly than those from a two-electrode chamber. A band width can be chosen that is more suitable for reducing the noise level, eliminating microphonics, increasing the permissible counting rate, and decreasing the building up of small background pulses. It is desirable to screen the collecting electrode as effectively as possible and at the same time to avoid the collection of electrons by the screening grid.

The present paper contains a theoretical and experimental study with the purpose of selecting a suitable grid and the proper operating voltages on the electrodes. The success of the arrangement is finally appraised by measuring the "line width" obtainable using a thin α-particle source.

Theoretical Analysis

(*a*) *Preliminary Statement*

A grid, G, shown in Fig. 1, is placed in front of the electron-collecting plate P to shield it from fields induced by the positive charges created at Q in the region A to G by ionization of a particle. It is convenient to define the electric field as the *positive* gradient of the potential, with the positive direction of the lines of force accordingly in the direction followed by electrons.

The efficiency of the grid shielding is measured by the extent to which the charge induced on P, or the number of lines per unit area ending there, E_P, is independent of the field E_Q. We define

$$\sigma = \frac{dE_P}{dE_Q}, \quad \text{for} \quad V_P - V_G = \text{constant}, \tag{1}$$

as the "inefficiency" of the grid, and calculate it as a function of the two geometrical ratios r/d and p/d (Fig. 1). The results are shown by Equation (14) and Fig. 3. The charge induced at P by a unit charge created at Q is then calculated in terms of σ and the distances AQ and AG (Equation (15)).

The proportion of electrons collected by the plate is roughly equal to the proportion of lines that by-pass the grid, as electrons diffuse along the lines of force at the pressures prevailing in an ionization chamber. (This was an initial assumption and is justified by the experimental work.) This proportion

is calculated in terms of the grid geometry and potentials (Fig. 4), and conditions are derived for which all the lines by-pass the grid (Equations (21) and (23)).

(*b*) *General Method*

For the purpose of calculation it is convenient to replace the grid by a fictitious conducting wall of thickness t held at a potential V_G' that differs from V_G by an amount ΔV depending on E_Q and E_P and the grid geometry (see lower part of Fig. 1).

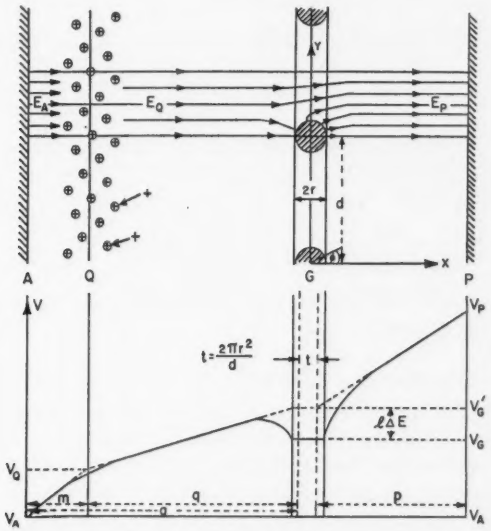

FIG. 1. *Field (upper) and potential (lower) in grid ionization chamber. Positive ions and electrons at Q are produced near the cathode A by α-particles. A grid G of parallel wires shields the electron collector P from induced effect of the positive ions.*

To calculate t, ΔV, the stagnation points (in the hydrodynamical sense), and numbers of lines, conformal representation theory is used (5). The number of lines passing between the x-axis and a general point in the x–y plane is denoted by U, the potential by V, and an analytic function of $z = x + iy$ is constructed to form the complex quantity $W = U + iV$. The grid wires are simulated by line charges and line dipoles placed along their axes. Nonuniformity of the field is neglected at P and Q. This assumption is permissible when their distances from the grid exceed the pitch of the grid wires.

(*c*) *Line Charges Induced in Grid Wires*

E_Q lines per unit area arrive at the grid, and E_P lines per unit area leave it. Hence $\Delta E = E_P - E_Q$ lines arise from unit area of grid or $(\Delta E)d$ lines from

a unit length of each wire, implying a line charge density of $(\Delta E)d/4\pi$ units. The complex potential function associated with unit line charge is $2i \log z$, but to represent the array of line charges producing a field periodic in y the function $\sinh \pi z/d$ must be used as argument of the logarithm in place of z. Now the equipotentials derived from the transformation

$$W = 2i \log \sinh \frac{\pi z}{d} \tag{2}$$

are approximately circular in the vicinity of $z = 0, \pm id, \pm 2\,id$, etc., and the mean value of the potential around an exact circle of radius r (the wire radius) is $2 \log \frac{\pi r}{d}$. Hence the complex potential

$$W_L = \frac{\Delta E}{2\pi} di \left(\log \sinh \frac{\pi z}{d} - \log \frac{\pi r}{d} \right) \tag{3}$$

takes account of the line charges induced in the wires when the grid is at zero potential. For large positive and negative x the potential is given approximately by

$$V_L = \frac{\Delta E}{2} \left(|x| - \frac{d}{\pi} \log \frac{2\pi r}{d} \right) + 0(e^{-2\pi|x|/d}). \tag{4}$$

The deviations from uniformity in the field are therefore small even when $|x|$ is of the same magnitude as d.

(d) Line Dipoles Induced in Grid Wires

A uniform field E induces a dipole of intensity $\frac{1}{2}Er^2$ at the center of a cylindrical conductor of radius r. It is reasonable to expect that the dipoles induced in the grid wires have the intensity $\frac{1}{2}\bar{E}r^2$, where $\bar{E} = (E_P + E_Q)/2$ is the mean of the distant fields on the two sides of the grid.

The complex potential function for line dipoles of unit strength, one at each wire position and all orientated in the x direction, is the derivative with respect to z of the unit line-charge function, i.e., $2\,i(\pi/d) \coth \pi z/d$. In accordance with our expectation, we use as a trial function

$$W_D = -\bar{E}r^2 i(\pi/d) \coth \pi z/d, \tag{5}$$

and show that when combined with the potential function representing the mean field, viz.,

$$W_E = i\bar{E}z, \tag{6}$$

it yields $|z| = r$ as zero equipotential. Neglecting terms of order r^3,

$$W_D + W_E = i\bar{E}\left(z - \frac{r^2}{z}\right) = -2\bar{E}r \sin \phi, \tag{7}$$

which is real as required. (The angle ϕ is measured from the x-axis.) Similarly $|z \pm nid| = r$ for $n = 1, 2, \ldots$ can be shown to be zero equipotentials.

(e) Complete Potential Function

The combination

$$W = iV_G + W_L + W_D + W_E \tag{8}$$

makes $|z| = r$, $|z \pm nid| = r$ equipotentials with $V = V_G$, and therefore satisfies conditions at the grid. It also yields correct values E_P and E_Q for the field at large positive and negative values of x. The function W yields

$$V = V_G + l(\Delta E) + E_P(x - \tfrac{1}{2}t) \tag{9}$$

and

$$V = V_G + l(\Delta E) + E_Q(x + \tfrac{1}{2}t) \tag{10}$$

for large positive and negative values of x respectively. In Equations (9) and (10)

$$l = \frac{d}{2\pi}\,(\tfrac{1}{4}\rho^2 - \log \rho), \tag{11}$$

$$t = \frac{d}{2\pi}\,\rho^2 = \rho r, \tag{12}$$

and

$$\rho = \frac{2\pi r}{d}\,. \tag{13}$$

More exact analysis reveals additional even powers of ρ in the formulas for l and t, beginning with

$$-\frac{7}{288}\left(\frac{d}{2\pi}\right)\rho^4 \quad \text{and} \quad -\frac{1}{12}\left(\frac{d}{2\pi}\right)\rho^4 \quad \text{respectively.}$$

These terms enter when, in order to make the equipotentials at the wires more nearly circular, quadrupoles are considered. The ratio l/d is plotted as a function of r/d in Fig. 2.

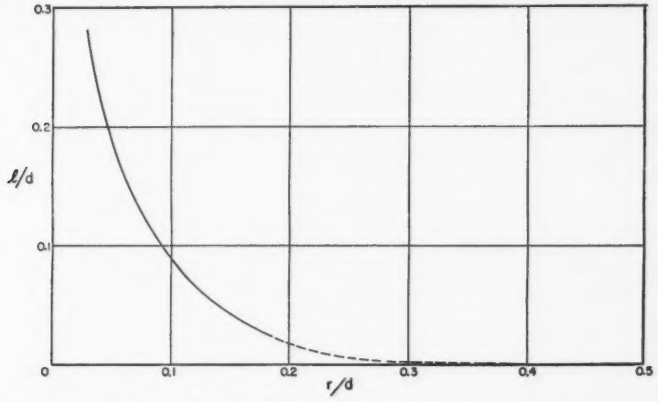

FIG. 2. *Curve of l/d as a function of r/d, which is convenient for calculating the inefficiency τ of a grid.*

(f) Inefficiency of Shielding

The inefficiency σ can be obtained by differentiating the relation

$$V_P - V_G = pE_P + l(\Delta E) = (p + l)E_P - lE_Q = \text{constant},$$

giving

$$\sigma = \frac{dE_P}{dE_Q} = \frac{l}{p + l} \approx \frac{d}{2\pi p} \log\left(\frac{d}{2\pi r}\right). \tag{14}$$

Curves of constant σ are shown in Fig. 3. It is seen that σ can be made small and the grid efficient either by choosing a grid-to-collector distance

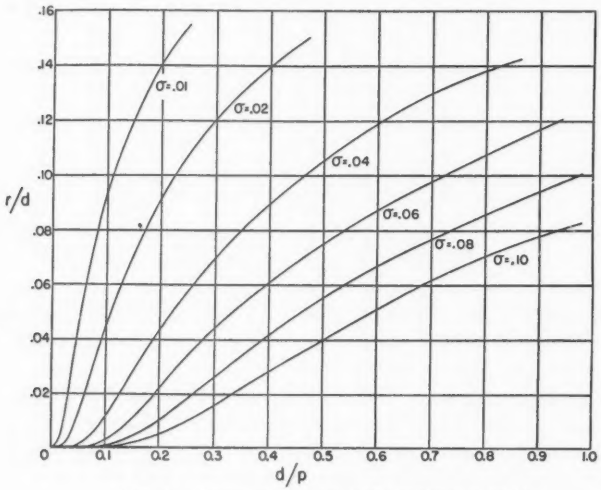

FIG. 3. *Curves of constant inefficiencies σ of grids.*

large compared to the pitch or by choosing the wire radius comparable to the pitch. It will be seen later that the second alternative is inadmissible (Equation (23)).

(g) Charge Induced at P by Charge Created at Q

From Fig. 1

$$V_G - V_A = mE_A + qE_Q - l(\Delta E)$$
$$= mE_A + (q + l)E_Q - lE_P = \text{constant}.$$

Therefore

$$mdE_A + (q + l)dE_Q - ldE_P = 0,$$

which with the relation

$$dE_P = \sigma dE_Q,$$

yields

$$\frac{\text{charge induced at } P}{\text{charge created at } Q} = -\frac{dE_P}{d(E_A - E_Q)}$$
$$= \frac{\sigma m}{a + l(1 - \sigma)} \approx \sigma \frac{\overline{AQ}}{\overline{AG}}. \tag{15}$$

(*h*) *Fraction of Lines Intercepted by Grid*

The real part U of the function W can be used to determine the number of lines leaving Q that are intercepted by the grid. On the grid wire where $|z| = r$ we obtain

$$U = -\phi(\Delta E)\frac{d}{2\pi} - 2\bar{E}r \sin\phi. \tag{16}$$

The stagnation points (5, p. 108), i.e., the points on the circumference where lines cease to enter and instead leave the grid, occur where U is stationary,

$$\text{i.e.,} \qquad \frac{\partial U}{\partial \phi} = 0.$$

Therefore

$$\cos\phi = -\frac{(\Delta E)}{2\bar{E}}\frac{d}{2\pi r} = -\frac{(\Delta E)}{2\rho\bar{E}}. \tag{17}$$

The number of lines collected by each wire from the field E_Q is given by the difference of U between the two solutions of (17) going via $\phi = \pi$. This difference is

$$\begin{aligned}\Delta U &= 4\bar{E}r\,|\sin\phi| - 2\,|\pi - \phi|\,(\Delta E)\frac{d}{2\pi} \\ &= 4\bar{E}r\sqrt{1 - \left(\frac{\Delta E}{2\bar{E}\rho}\right)^2} - 2(\Delta E)\frac{d}{2\pi}\cos^{-1}\left(\frac{\Delta E}{2\bar{E}\rho}\right).\end{aligned} \tag{18}$$

The number of lines collected by unit area of the grid is $\Delta U/d$, and the ratio between this and E_Q represents the grid loss λ:

$$\lambda = \frac{\Delta U}{E_Q d} = \frac{E_P - E_Q}{\pi E_Q}\left\{\sqrt{\left(\frac{E_P + E_Q}{E_P - E_Q}\rho\right)^2 - 1} - \cos^{-1}\left(\frac{E_P - E_Q}{E_P + E_Q}\frac{1}{\rho}\right)\right. \tag{19}$$

The proportion of lines that end on the collector rather than the grid, $1 - \lambda$, is plotted as a function of E_P/E_Q for three values of ρ in Fig. 4 over the range where the square root and the inverse cosine are real, viz.,

$$\frac{1-\rho}{1+\rho} < \frac{E_P}{E_Q} < \frac{1+\rho}{1-\rho}. \tag{20}$$

The ends of the interval correspond to the conditions where the stagnation points unite and slip off the wires in the direction of the weaker field. For

$$\frac{E_P}{E_Q} > \frac{1+\rho}{1-\rho} \tag{21}$$

all lines by-pass the grid, and $1 - \lambda = 1$. For

$$\frac{E_P}{E_Q} < \frac{1-\rho}{1+\rho} \tag{22}$$

all of the balance between E_Q and E_P is collected by the grid,

$$\lambda = \frac{E_Q - E_P}{E_Q} \qquad \text{and} \qquad 1 - \lambda = \frac{E_P}{E_Q}.$$

Since V_G' differs from V_G, E_P/E_Q is not strictly proportional to the grid-plate potential difference for fixed $V_G - V_A$. Deviations from proportionality are of the order of σ. In particular zero grid-collector potential difference corresponds to $E_P/E_Q = \sigma$. The origin must be shifted to the right by an amount σ in Fig. 4 if the abscissa is to become a more accurate measure of the grid-collector potential difference (broken line).

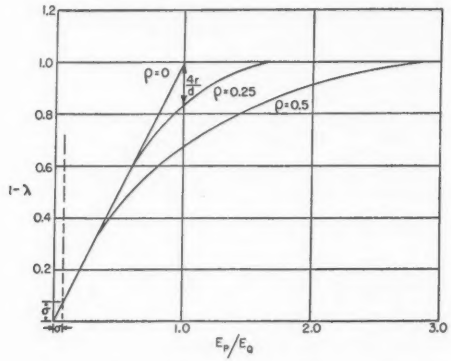

FIG. 4. *Fraction of lines from cathode that end on electron collector is plotted against the field ratio E_P/E_Q. The origin must be shifted by σ if $(V_P - V_G)/p$ is used for E_P. ($\rho = 2\pi r/d$).*

(i) Condition on Potential Differences for Zero Grid Interception

Condition (21) applies when all lines by-pass the grid. If this condition is satisfied in the absence of positive charge at Q, then it will certainly be satisfied in the presence of such charge. Hence a sufficient condition on V_A, V_P, and V_G can be derived on the assumption that there is no charge at Q. Substitution for E_P and E_Q then gives the condition:

$$\frac{V_P - V_G}{V_G - V_A} \geqslant \frac{p + p\rho + 2l\rho}{a - a\rho - 2l\rho}. \tag{23}$$

This must be balanced against the condition that σ (or l/p) should be small for efficient shielding (Equation (14)).

Experimental Investigation

An experimental investigation was undertaken to test the main results from the theoretical analysis and to indicate what lower limit in width of an α-particle line might be realized in practice.

(a) Ionization Chamber

The ionization chamber consisted of two parallel plates, 10 cm. square and about 6 cm. apart, mounted on insulators inside a cylindrical vessel. The

gas was argon, usually at a pressure of 3 atm. A grid of parallel wires could be mounted 1.43 or 0.67 cm. in front of the collector. Two grids were tested; one consisted of No. 38 copper wires 0.20 cm. apart, and the other of No. 36 copper wires 0.091 cm. apart. A negative potential of 1200 v. was applied to the cathode, which produced an adequate field between the electrodes for electron collection.

Sources of α-particles were made by evaporating a solution of polonium 210 on gold foils. The source, covered by a collimator consisting of $\frac{1}{8}$ in. holes in a 1/32 in. aluminum sheet, was placed against the cathode. Without the collimator the distribution of pulse sizes was not symmetrical about the maximum and had a tail on the low energy side. This distortion is attributed to α-particles that had traveled approximately in the plane of the source and lost energy in irregularities in the source or in the backing foil before being scattered into the gas.

The electronic equipment for the measurement of pulse size has been described (1). The ionization pulses at the collector were fed into an amplifier designed for low noise and high stability of gain and then into a cutoff amplifier that subtracted a predetermined voltage and amplified the remainder. The output pulses were electronically sorted into groups according to height by a pulse analyzer (3). In this way the "line" containing the pulse heights could be expanded to show its shape and thereby to yield quantitative information on width at half-maximum or alternatively on the standard deviation from the mean.

(b) Collection of Electrons by the Grid

The first point considered was the possible collection of electrons by the grid. This is undesirable for two reasons. (1) The pulse size and the signal-to-noise ratio would be reduced. (2) The fraction of electrons collected might depend somewhat on the track orientation, and thus an additional cause of spread might enter.

Fig. 4 shows the fraction of lines from the cathode which by-pass the grid and end on the collecting electrode. If the electrons diffuse along the lines of force these relations also give the fractions of charge reaching the collecting electrode. Fig. 5 shows two curves of observed pulse size plotted against the ratio of the fields on the two sides of the grid. Figs. 4 and 5 are in good agreement, particularly at the upper end. For this region the field lines are nearly straight in the chamber. For very low potential difference between grid and collector the field lines have considerable curvature, and agreement is not as good. The pulses are larger than those calculated; this suggests that electrons slip off the field lines and reach the collector. The intercept for zero potential difference between grid and collector is greater than σ. It is seen

in Fig. 5 that a voltage can be chosen for the grid at which it does not collect electrons. The chamber is ordinarily operated under this condition.

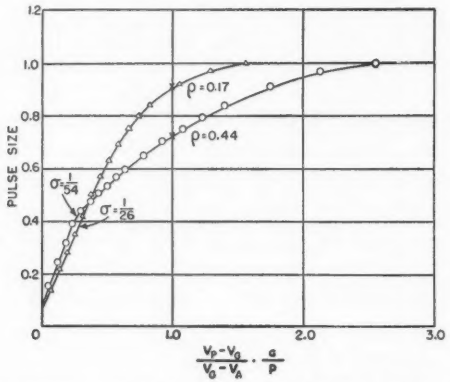

FIG. 5. *Observed pulse size, indicating fraction of electrons reaching the collector, is plotted against* $\frac{V_P - V_G}{V_G - V_A} \cdot \frac{a}{p}$ *(Grids Nos. 2 and 3). The two points marked by crosses were calculated from theory.*

(c) Spread of Pulse Size

Table I and Fig. 6 show the results of a typical run with polonium α-particles. The distribution of pulses from a signal generator is included. The distribution of the α-particle pulses is approximately Gaussian having a standard deviation s_1. Five causes of spread may be noted: (1) thickness of source

TABLE I

PULSE DISTRIBUTIONS FOR α-PARTICLES AND ARTIFICIAL SIGNALS

Pulse analyzer channel No.	α-particles, counts	Artificial pulses, counts
1	0	—
2	2	—
3	2	—
4	2	—
5	4	—
6	4	—
7	8	—
8	8	—
9	8	—
10	10	2
11	20	10
12	48	96
13	64	158
14	116	162
15	124	66
16	116	20
17	48	—
18	14	—
19	2	—

material, (2) straggling of ionization, (3) variation of rise time of the electron pulses, (4) noise of the amplifier, and (5) induced effect of positive ions, as described in the introduction. The last item will be referred to as spread

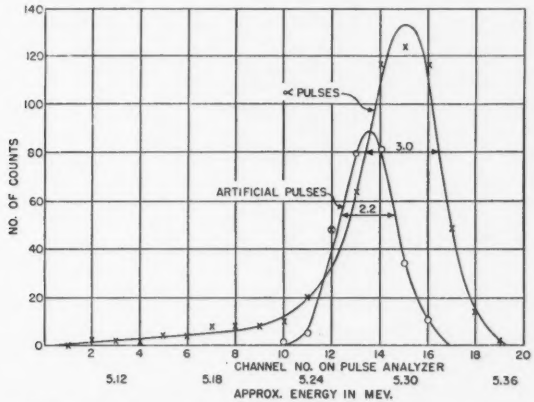

FIG. 6. *Typical distributions of pulse sizes for polonium α-particles and artificial pulses (Grid No. 1). One channel spacing on pulse analyzer is equal to 15 kev.*

caused by the chamber. The observed standard deviation s_1 is assumed to be associated with the separate standard deviations s_a, s_i, s_r, s_n, and s_c from the above causes respectively by the formula:

$$s_1 = \sqrt{s_a^2 + s_i^2 + s_r^2 + s_n^2 + s_c^2}\,.$$

In the present experiments s_a, s_i, and s_r always occur together, while s_n can be obtained by using artificial pulses. It is intended to compare the values of s_c obtained from measurements with the various grids with the theory.

(d) Spread of Pulse Size Due to Chamber

The distribution of pulse size will be examined, the effect of orientation of the α-particle track being taken into account. Noting that the induced effect of the positive ions depends on the first power of m (Equation (15)), the idea of center of ionization may be introduced (similar to center of mass in mechanics). The effective range $\bar{R}$, measured from the source of the α-particle to the center of ionization in the track, is evaluated from the Bragg curve for a single polonium α-particle. The perpendicular distance from the center of ionization to the cathode may be taken as the value of m.

The centers of ionization possess a distribution of m's for a point source of α-particles at O in Fig. 7, without a collimator, having limits zero and $\bar{R}$. If N α-particles are emitted isotropically, the number making angles between θ and $\theta + d\theta$ with the normal is

$$\frac{2\pi N\bar{R}^2 \sin\theta\, d\theta}{4\pi\bar{R}^2} = \frac{N}{2}\sin\theta\, d\theta = \frac{Ndm}{2\bar{R}}\,.$$

Thus, the distribution of m's is rectangular (extending from $m = 0$ to $m = \bar{R}$), giving a similar distribution of pulse sizes. The maximum pulse size is that for which $m = 0$ and the minimum is that for which $m = \bar{R}$. In the absence of a

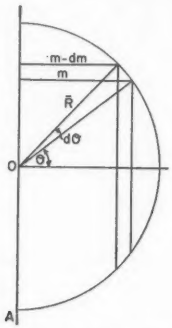

FIG. 7. *Source at point O emits α-particles of effective range $\bar{R}$ measured from O to centers of ionization in tracks.*

grid the fractional width of the pulse distribution is equal to $\bar{R}$/(separation of electrodes). Fig. 8 shows pulse distributions observed without a grid. The

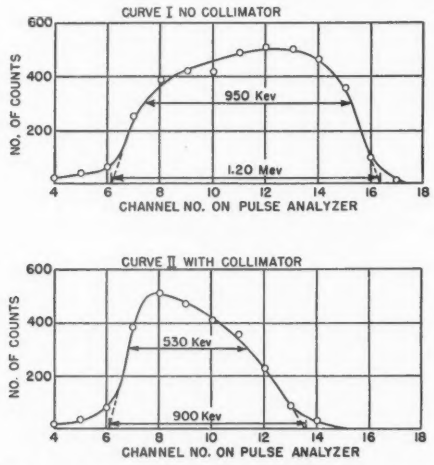

FIG. 8. *Observed distributions of α-particle pulses in ionization chamber without a grid. Separation of electrodes was 5.9 cm. Argon pressure was 2 atm. Effect of collimator is shown.*

effective range $\bar{R}$ was calculated to be 1.15 cm. in argon at 2 atm., and the separation of electrodes was 5.9 cm. Thus the expected width of the pulse distribution of polonium α-particles without a collimator is $\frac{1.15}{5.9} \times 5.30$ Mev. = 1.0 Mev., in fair agreement with that observed (Curve I, Fig. 8).

When a collimator is used the distribution of pulse size is changed, as shown in Fig. 8. The collimator cuts off the largest pulses, which must come from the tracks making small angles with the cathode, since the induced effect of the positive ions is least for these tracks. The width at 60.7% of the maximum is reduced by the factor 950/530 = 1.8. The calculated reduction is about 2.5. Since neither distribution is Gaussian, the first being rectangular, and the second nearly triangular, the exact value chosen for the effect of the collimator is rather arbitrary. The standard deviation when the collimator is present is about $\frac{1}{2}$ (530) kev. This may be related to the energy 5.30 Mev. of the polonium α-particle as follows:

$$\text{Standard deviation} = \frac{1}{2}\left(\frac{\bar{R}}{5.9f}\right) 5300 \text{ kev.} = \frac{1}{2}\,(530) \text{ kev.},$$

where f is the collimator factor. Using $\bar{R} = 1.15$ cm. it is found that $f = 2.0$. It will be seen later that with a good grid shielding the collector the spread due to the chamber is not as large as other spreads. Therefore the distribution of pulse size with a spread due only to the chamber may be assumed Gaussian, and the collimator factor 2.0 carried over into the corresponding standard deviation.

(e) Shielding by the Grid

The standard deviation of a pulse distribution was estimated by three methods (6, pp. 134-153). (1) The width of the peak was measured at 60.7% of the maximum. (2) The mean square deviation was obtained from the histogram and Sheppard's correction applied. (3) An ogive plot, such as shown in Fig. 9, was used. The last method appeared most reliable. For

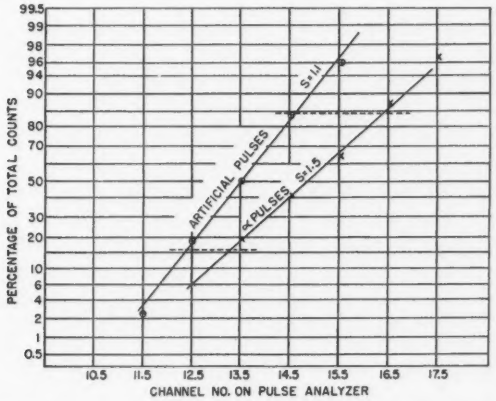

FIG. 9. *Ogive plot for estimating standard deviation of a pulse distribution. Standard deviation is half of number of channels between intersections at dotted lines.*

the data in Table I the standard deviations are 1.5 and 1.1 channel widths of the pulse analyzer respectively for the α-particles and artificial pulses.

Table II summarizes the experimental results for four different grid arrangements. The inefficiencies σ were calculated from Equation (14). The standard deviations are the averages of five determinations in each case. The small variations in s_n observed for the different experimental arrangements are in approximate agreement with the expected effects of changing the capacity of the chamber.

TABLE II

STANDARD DEVIATIONS IN PULSE DISTRIBUTIONS

s_1 = standard deviation for α-particle pulses
s_2 = standard deviation for artificial pulses
1 channel spacing = 15 kev.

Grid No.	$\sigma \times 10^3$	s_1, channels	s_2, channels	$\sqrt{s_1^2 - s_2^2}$, channels	$\sqrt{s_1^2 - s_2^2}$, kev.
1	8.73	1.42	1.08	0.92	13.8
2	18.5	1.66	1.25	1.09	16.4
3	38.3	1.65	1.05	1.27	19.1
4	78.4	1.74	1.10	1.35	20.2
4*a*	78.4	2.40	1.10	2.13	32.0

Grid No. 1: $r = 6.35 \times 10^{-3}$ *cm.,* $d = 0.091$ *cm.,* $p = 1.43$ *cm.,* $AG = 4.49$ *cm.,* $\bar{R} = 0.77$ *cm. (argon at 3 atm. pressure).*

Grid No. 2: $r = 6.35 \times 10^{-3}$ *cm.,* $d = 0.091$ *cm.,* $p = 0.67$ *cm.,* $AG = 4.93$ *cm.,* $\bar{R} = 0.77$ *cm.*

Grid No. 3: $r = 5.34 \times 10^{-3}$ *cm. (wire coated with Aquadag),* $d = 0.20$ *cm.,* $p = 1.43$ *cm.,* $AG = 4.49$ *cm.,* $\bar{R} = 0.77$ *cm.*

Grid No. 4: $r = 5.34 \times 10^{-3}$ *cm.,* $d = 0.20$ *cm.,* $p = 0.67$ *cm.,* $AG = 4.93$ *cm.,* $\bar{R} = 0.77$ *cm.*

Grid No. 4a: same as No. 4 except that $\bar{R} = 1.15$ *cm. in argon at 2 atm. pressure.*

For the α-particle pulses

$$s_1 = \sqrt{s_s^2 + s_i^2 + s_r^2 + s_n^2 + s_c^2} ,$$

and for the artificial pulses

$$s_2 = \sqrt{s_n^2} .$$

Therefore

$$\sqrt{s_1^2 - s_2^2} = \sqrt{s_s^2 + s_i^2 + s_r^2 + s_c^2} .$$

The squares of the standard deviations s_s, s_i, and s_r, caused by the thickness of the source, straggling of ionization, and variations in rise time, should form an approximately constant quantity, independent of the grid. The standard deviation s_c caused by the chamber is expected to be

$$s_c = \frac{\sigma \bar{R}}{2f(a + l(1 - \sigma))} 5300 \text{ kev.} = \eta \times 5300 \text{ kev.}$$

from Equation (15) and the effect of the collimator. Owing to the finite extent of the electrodes and the proximity of the wall of the surrounding vessel one might expect s_c to be merely proportional to this expression. Although the constant of proportionality turned out to be approximately unity, at first proportionality but not equality was assumed. The measured quantities $\sqrt{s_1^2 - s_2^2}$ given in Table II were set equal to $\sqrt{a + b\eta^2}$. The best values of the parameters a and b, assumed to be constants, were obtained by the method of least squares, with the following result:

$$\sqrt{a} = \sqrt{s_s^2 + s_i^2 + s_r^2} = 14.3 \text{ kev.}$$

and

$$\sqrt{b} = 6030 \text{ kev.}$$

Table III shows that a satisfactory fit of all experimental data was obtained. The predicted shielding by the grid is verified, as shown by $\sqrt{b} = 6030$ kev. being approximately equal to the expected 5300 kev. or alternatively by the agreement of Columns 5 and 6. The discrepancy involves f directly, which is difficult to estimate owing to the asymmetry of the pulse distribution, as pointed out above.

TABLE III

STANDARD DEVIATIONS CAUSED BY CHAMBER

Grid No.	$\eta \times 10^4$	$\sqrt{s_1^2 - s_2^2}$, kev. (observed)	$\sqrt{s_s^2 + s_i^2 + s_r^2 + s_c^2}$, kev. (least squares)	s_c, kev. (least squares)	$\eta \times 5300$ kev. (theory)
1	3.74	13.8	14.5	2.2	2.0
2	7.19	16.4	15.0	4.3	3.8
3	16.25	19.1	17.3	9.8	8.6
4	30.3	20.2	23.2	18.3	16.1
4a	45.3	32.0	30.8	27.3	24.0

The following consideration shows that the standard deviation s_r is relatively small. This cause of spread in pulse size is the variation in electron collection times due to different orientations of the tracks of the α-particles. The band width of the amplifier used was defined by the usual two time constants of smoothing and differentiation, which were adjusted to be 5 and 50 μsec. respectively. The collection time is not known with certainty, but a rough measurement was made by decreasing the time constants of the amplifier to 1 and 10 μsec. There was no appreciable drop in pulse amplitude, which indicates a collection time of about 1 μsec. With time constants of 5 and 50 μsec. a variation in collection time between zero and 2 μsec. would introduce a *total* spread of only 4 kev., which is much smaller than the spreads introduced by source thickness and ionization straggling.

(f) Limitations on Standard Deviations

The standard deviation from all causes on the pulse distribution of polonium α-particles was found to be as low as 22 kev. when a suitable grid was placed

in front of the electron collector. The corresponding width of the line at half-maximum was 50 kev. or about 1% of the energy of the polonium α-particle. The standard deviation caused by the induced effect of the positive ions was found to be as low as 2 kev. when a carefully designed grid was used to shield the collector. This cause of spread is now negligible, and further decrease in line width can be effected only by attention to other causes.

Through the use of artificial pulses the standard deviation caused by noise in the head amplifier was found to be about 17 kev. With existing tubes not much improvement can be expected here. The standard deviation caused by thickness of source, straggling of ionization, and variations in rise time of the pulses was 14 kev. From Fano's theory (2) an estimate of the standard deviation caused by straggling of ionization is about 8 kev. With the best conditions an over-all standard deviation of about 18 kev. may perhaps be attained. This corresponds to a width of 45 kev. at half-maximum for the polonium α-particle line.

Acknowledgments

We wish to thank Dr. B. W. Sargent and Mr. G. C. Hanna for their assistance and criticisms in preparing this paper for publication.

References

1. CRANSHAW, T. E. and HARVEY, J. A. Can. J. Research, A, 26 : 243. 1948.
2. FANO, U. Phys. Rev. 72 : 26. 1947.
3. FREUNDLICH, H. F., HINCKS, E. P., and OZEROFF, W. J. Rev. Sci. Instruments, 18 : 90. 1947.
4. FRISCH, O. R. Unpublished report, BR-49. Isotope analysis of uranium samples by means of their α-ray groups. British Atomic Energy Project.
5. SHOTTKY, W. (Part IIA) and POHLHAUSEN, K. (Part IIB). Theory of functions as applied to engineering problems. *Edited by* R. Rothe, F. Ollendorff, and K. Pohlhausen. Technology Press, Massachusetts Institute of Technology, Cambridge, Mass., U.S.A.
6. YULE, G. U. and KENDALL, M. G. An introduction to the theory of statistics. Charles Griffin & Co. Ltd., London, England. 1940.

CANADIAN JOURNAL OF RESEARCH

Notes on the Preparation of Copy

GENERAL:—Manuscripts should be typewritten, double spaced, and the **original and one extra copy** submitted. Style, arrangement, spelling, and abbreviations should conform to the usage of this Journal. Names of all simple compounds, rather than their formulae, should be used in the text. Greek letters or unusual signs should be written plainly or explained by marginal notes. Superscripts and subscripts must be legible and carefully placed. Manuscripts should be carefully checked before being submitted, to reduce the need for changes after the type has been set. If authors require changes to be made after the type is set, they will be charged for changes that are considered to be excessive. **All pages, whether text, figures, or tables, should be numbered.**

ABSTRACT:—**An abstract of not more than about 200 words, indicating the scope of the work and the principal findings, is required.**

ILLUSTRATIONS:

(i) *Line Drawings:*—All lines should be of sufficient thickness to reproduce well. Drawings should be carefully made with India ink on white drawing paper, blue tracing linen, or co-ordinate paper **ruled in blue only**; any co-ordinate lines that are to appear in the reproduction should be ruled in black ink. Paper ruled in **green, yellow, or red should not be used** unless it is desired to have all the co-ordinate lines show. Lettering and numerals should be neatly done in India ink preferably with a stencil (**do not use typewriting**) and be of such size that they will be legible and not less than one millimeter in height when reproduced in a cut three inches wide. All experimental points should be carefully drawn with instruments. Illustrations need not be more than two or three times the size of the desired reproduction, but the ratio of height to width should conform with that of the type page. **The original drawings and one set of small but clear photographic copies are to be submitted.**

(ii) *Photographs:*—Prints should be made on glossy paper, with strong contrasts; they should be trimmed to remove all extraneous material so that essential features only are shown. Photographs should be submitted **in duplicate**; if they are to be reproduced in groups, one set should be so arranged and mounted on cardboard with rubber cement; the duplicate set should be unmounted.

(iii) *General:*—**The author's name, title of paper, and figure number should be written in the lower left-hand corner (outside the illustration proper) of the sheets on which the illustrations appear.** Captions should not be written on the illustrations, but typed on a separate page of the manuscript. All figures (including each figure of the plates) should be numbered consecutively from 1 up (arabic numerals). **Each figure should be referred to in the text.** If authors desire to alter a cut, they will be charged for the new cut.

TABLES:—Titles should be given for all tables, which should be numbered in Roman numerals. Column heads should be brief and textual matter in tables confined to a minimum. **Each table should be referred to in the text.**

REFERENCES:—**These should be listed alphabetically by authors' names, numbered in that order, and placed at the end of the paper.** The form of literature citation should be that used in the respective sections of this Journal. **Titles of papers should not be given in references listed in Sections A, B, E, and F, but must be given in references listed in Sections C and D.** The first page only of the references cited in papers appearing in Sections A, B, and E should be given. **All citations should be checked with the original articles.** Each citation should be referred to in the text by means of the key number; in Sections C and D the author's name and the date of publication may be included with the key number if desired.

The *Canadian Journal of Research* conforms in general with the practice outlined in the *Canadian Government Editorial Style Manual*, published by the Department of Public Printing and Stationery, Ottawa.

Reprints

Fifty reprints of each paper without covers are supplied free. Additional reprints, if required, will be supplied according to a prescribed schedule of charges. On request, covers can be furnished at cost.